Solar Energy Materials & Solar Cells 98 (2012) 277–282

Contents lists available at SciVerse ScienceDirect

Solar Energy Materials & Solar Cells

journal homepage: www.elsevier.com/locate/solmat

Low cost high-efficiency amorphous silicon solar cells with improved light-soaking stability

Jung Y. Huang [a,*], Chien Y. Lin [a], Chang-Hong Shen [b], Jia-Min Shieh [b], Bau-Tong Dai [b]

[a] Department of Photonics and Institute of Electro-Optical Engineering, Chiao Tung University, 30020, Taiwan
[b] National Nano Device Laboratories, No. 26, Prosperity Road 1, Hsinchu 30078, Taiwan

ARTICLE INFO

Article history:
Received 20 June 2011
Received in revised form
19 October 2011
Accepted 14 November 2011
Available online 1 December 2011

Keywords:
Solar cell
Amorphous silicon
Thin film photovoltaics
Light soaking

ABSTRACT

We investigate the performance of amorphous Si (a-Si) solar cells fabricated with Inductively Coupled Plasma (ICP) deposition technique. The ICP system produces a-Si films with low defect density (3×10^{15} cm^{-3}), resulting in a conversion efficiency of 9.6%. Deep level transient spectroscopy (DLTS) reveals that hole carriers trapped at defects near the valence band edge delocalize at 130 K; while trapped electrons can only be emitted into the conduction band near room temperature. Spectrally resolved DLTS study further indicates that light soaking enhances the emission rate of the tapped electrons near the conduction band edge while reduces the transition moments from the hole-trapping defect levels to the conduction band. The combined effects and light soaking-induced defects are responsible for the degradation of a thin film solar cell by light soaking.

1. Introduction

Photovoltaic (PV) technology is attractive for its potential to solve our energy security issue by serving as the major carbon-free renewable energy source. Thanks to the long-term efforts in microelectronic industry, silicon-based PV technology has reached a state-of-the-art status. However, currently single-crystal solar cells remain much more expensive than thin-film devices, which significantly limits its wide spread use. Hydrogenated amorphous silicon (a-Si:H) is well suited for PV applications [1,2]. To promote the wide spread use of thin film PV technology, two obstacles have to be overcome. First, a low cost deposition technique must be developed to fabricate high-efficiency thin film PV devices. Secondly, prolonged light exposure induced degradation has to be minimized to further improve long-term reliability of thin film PV devices [3–5].

Capacitor-type plasma-enhanced chemical vapour deposition (PECVD) generates abundant short-life radicals, which eventually form weak bonding configuration in a-Si:H films [5–7]. Light exposure on the a-Si:H can move the hydrogen atoms of the weak bonding configurations and create new dangling bonds [5,7], resulting in poor reliability of the devices. There has been a growing interest in CVD technique with high-density plasma (HDP) source because HDP CVD offers the possibility of improved film quality at reduced process temperatures [8–11]. Inductively coupled plasma chemical vapour deposition (ICP CVD) technique [12,13] possesses high fractional ionization capacity, therefore high-density plasma can be produced to improve diffusion of the reactive radicals on a substrate at fairly low deposition temperatures. ICP CVD can also reduce the ion bombardment on the growing surface and yields a film with low density of defects. Recently, we found that thin dielectric films prepared with an ICP reactor possess low level of hydrogen inclusion and carrier trapping sites [14]. Significant efforts have also been made to improve the uniformity of ICP for mass deposition of large-area films [15–19]. It is expected that ICP CVD could yield semiconductor films with good carrier transport property and a robust lattice framework that is more resistant to light exposure. However, potential use of ICP grown semiconductor films for PV application is not clear. In this study, we verified this expectation by demonstrating single-junction ICP CVD a-Si solar cells with a conversion efficiency of 9.6% and improved light-soaking stability. The electrical characteristics, defect density and light soaking behaviour of ICP CVD films had been measured and discussed in detail to facilitate further development of this thin film technique for PV application.

2. Experimental methods

2.1. Materials synthesis and device fabrication

From the growth mechanism of thin film with ICP CVD, increasing ICP power typically leads to an increase of deposition rate. Because of the high surface mobility of reactive species in

* Corresponding author. Tel.: +886 3 5731975; fax: +886 3 5716631.
E-mail addresses: jyhuang@faculty.nctu.edu.tw (J.Y. Huang), jmshieh@ndl.narl.org.tw (J.-M. Shieh).

0927-0248/$ - see front matter © 2011 Elsevier B.V. All rights reserved.
doi:10.1016/j.solmat.2011.11.023

ICP, we can synthesize films slowly to yield denser framework with low hydrogen content by using low ICP power and high substrate temperature.

In our ICP CVD system, the reactor is a stainless-steel cylinder with a diameter of 45 cm and a height of 50 cm. The plasma was generated inductively by a radio frequency (RF) power source of 13.56 MHz connected to a copper coil placing outside of a ceramic tube in the deposition chamber. During the deposition, hydrogen dilution ratio $[H_2]/[SiH_4]$ and working gas pressure were kept at 10 and 700 m-Torr, respectively. Hydrogenated amorphous Si films can be deposited on a substrate at 140 °C with a RF power density of 135 mW/cm^2. The deposition rate of a-Si:H film with ICP CVD is about 0.3 nm/s. For comparison, we also prepared a-Si:H films at 140 °C with a VHF-PECVD system operating at 40 MHz with power density of 83 mW/cm^2. Similar dilution ratio and total working gas pressure were used. The deposition rate of VHF-PECVD a-Si:H film is about 0.1 nm/s. Relevant growth parameters and material properties of the thin films deposited by the two methods are summarized in Table 1.

Table 1
Growth parameters and material properties of a-Si thin films by ICP-CVD and VHF-PECVD.

Parameters	ICP-CVD	VHF-PECVD
Deposition rate (nm/s)	0.3	0.1
Deposition temperature (°C)	140	140
Dilution ratio of H_2: $[H_2]/[SiH_4]$	10	10
Working gas pressure (m-Torr)	700	700
n-i-p-Layer thickness (nm)	20–400–12	20–400–12
Energy bandgap (eV)	1.85	1.90
Cell dimension	1 cm × 1 cm	1 cm × 1 cm

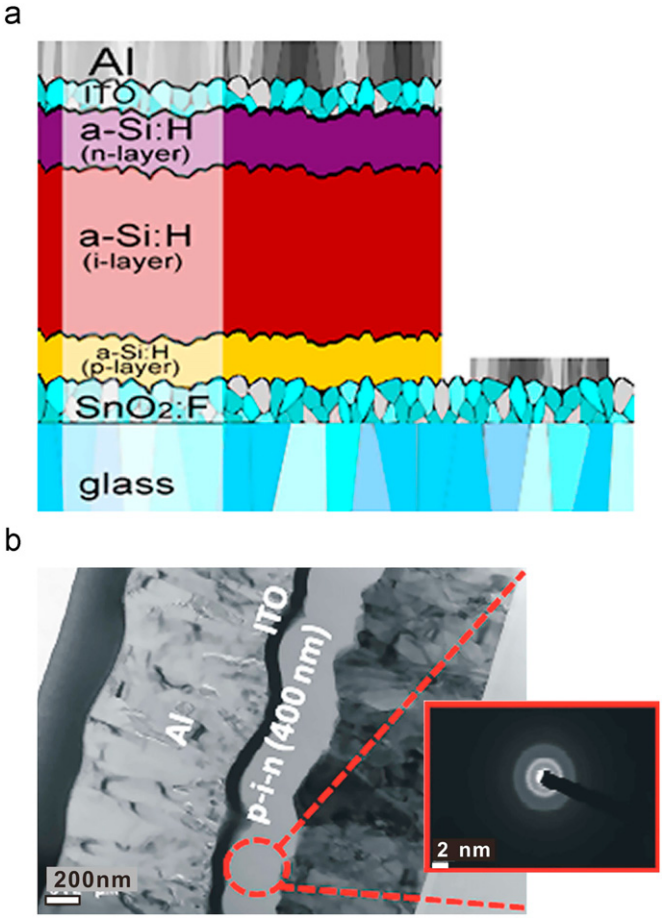

Fig. 1. (a) Schematic diagram showing the device structure of an a-Si pin solar cell. (b) The cross-sectional TEM image showing the a-Si pin solar cell fabricated by ICP CVD on Asahi U substrate. Spatially resolved diffraction pattern of the a-Si pin stack reveals clearly the amorphous phase.

To fabricate a-Si:H solar cells with a schematic structure shown in Fig. 1(a), we first deposited a p-i-n stack on Asahi substrates (SnO_2 : F/glass) by ICP CVD or VHF-PECVD. The dimensions of the test cells are 1 cm × 1 cm. The thickness of the intrinsic layers in the test cells was kept at 400 nm. Doped layers with thickness of 12 nm (p-layer) or 20 nm (n-layer) were synthesized with an admixture of either 10% B_2H_6 (p-layer) or 3% PH_3 (n-layer). A reflective contact of indium-tin-oxide (ITO)/Al was then deposited by DC-sputtering on the back side to yield efficient light trapping. The ITO layers have high electrical conductivity ($< 1 \times 10^{-3}$ ohm cm) and optical transmittance ($> 90\%$, 400−900 nm), which significantly improve the light transmission and reduce the series resistance of the devices. The cross-sectional transmission electron microscopy (TEM) image of an a-Si solar cell and the spatially resolved diffraction pattern at the p-i-n stack are presented in Fig. 1(b), which clearly indicates an amorphous phase for the pin stack.

2.2. Characterization techniques

2.2.1. Performance assessment and light-soaking test of a-Si pin solar cells

We characterized the PV performance of a solar cell by first measuring the current density–voltage (J–V) characteristics and the external quantum efficiency spectrum with an AM1.5G light source (Global sun simulator Oriel Sol3A). The accelerated light-soaking tests were then performed by using an AM1 white light source with an irradiance of 600 mW/cm^2 (six-Sun). During the light-soaking measurements, the device under test was not temperature-controlled. The device temperature can rapidly reach steady state at 60 °C. Therefore, the condition of our light soaking can be considered to be irradiated with six Suns at 60 °C.

2.2.2. Deep-level transient spectroscopy (DLTS) and spectrally resolved DLTS of a-Si pin solar cells

Free carriers in the i-layer region of a pin diode at reverse bias are very low. Thus, the occupation probability of a defect level at E_t in the energy bandgap can be expressed as

$$P(E_t) = \frac{c_n n + e_p}{c_n n + e_p + c_p p + e_n} \simeq \frac{e_p}{e_p + e_n}, \quad (1)$$

where c_p (c_n) denotes the capture cross section of the trap defect for hole (electron) and e_p (e_n) is the hole (electron) emission rate of the trap level. The electron (hole) emission process becomes dominant when the trap level lies in the upper (lower) half of the bandgap. At forward bias, free carriers are abundant in the i-layer, yielding an occupation probability $P(E_t) = c_n n/(c_n n + c_p p)$. Thus, the trap levels lying in the upper half of the bandgap can be filled with electrons by using a forward-biasing pulse. After the device returns to the reverse bias condition, the trapped electrons will be released to the conduction band, leading to a transient capacitance change. The traps lying in the lower half of the bandgap with $c_p \gg c_n$ can be detected with a similar process. This can be understood by looking at the forward bias condition,

$$1 - P(E_t) = 1 - \frac{c_n n}{c_n n + c_p p} = \frac{c_p p}{c_p p + c_n n} = \frac{1}{c_n/c_p + 1} \to 1 \quad (2)$$

implying that donor defect levels can be effectively filled with holes during the filling pulse. However, the situation is more complex for the defect levels with $c_p < c_n$, because these defects cannot be filled effectively with holes during the filling pulse. In this case, different filling scheme shall be implemented.

The sample under test with deep level transient spectroscopy (DLTS) is first reversely biased. A pulse with appropriate duration is then repetitively superimposed on the DC level to forwardly bias the device in a brief duration. During the brief forward-biasing period, charge carriers are injected from both sides of the semiconductor junction into trap levels. Once the pulse is removed, the trapped carriers will be removed by emitting to the conduction/valence band with an emitting rate e_n (or e_p), which depends on the sample temperature. Thus, a transient capacitance change after the injection pulse can be observed [20]. The capacitance of the device under reverse bias V_r is given by

$$C_0 = A\sqrt{\frac{\varepsilon_r\varepsilon_0 eN_i}{2(V_r+V_{bi})}}. \quad (3)$$

Here A is the device area and V_{bi} the built-in voltage. Assuming a trap level of concentration N_t in the sample, the capacitance change under a reverse bias V_r becomes

$$\Delta C(t) = C(t)-C_0 = A\sqrt{\frac{\varepsilon_r\varepsilon_0 e[N_i+N_t(t)]}{2(V_r+V_{bi})}}-A\sqrt{\frac{\varepsilon_r\varepsilon_0 eN_i}{2(V_r+V_{bi})}} \approx \frac{N_t}{2N_i}C_0 \quad (4)$$

as $N_t \ll N_i$. We measured the transient capacitance curve $\Delta C(t)$ with HP4280A capacitance meter under computer control.

As pointed out above, defect levels with $c_p < c_n$ cannot be effectively filled with holes during the filling pulse. To circumvent this difficulty, we label these defect levels with optical transition by using light with appropriate optical frequency. Following Eq. (3), we can derive the capacitance $C_{light}(t)$ of a pin device irradiated with light of a photon energy E_ω as

$$C_{light}(t) = A\sqrt{\frac{\varepsilon_r\varepsilon_0 e[N_i+N_t(t)+N_t(t,E_\omega)]}{2(V_r+V_{bi})}} \quad (5)$$

with $N_t(t)$ denoting the number of defects with trapped carriers from injection and $N_t(t, E_\omega)$ the number of defects being labelled by optical transition. If $N_t \ll N_i$, the spectrally resolved transient capacitance change can then be approximated as

$$C_{light}(t)-C_{dark}(t) \approx \frac{N_t(t,E_\omega)}{2N_i}C_0 \quad (6)$$

with $C_{dark}(t) = A\sqrt{(\varepsilon_r\varepsilon_0 e[N_i+N_t(t)])/(2(V_r+V_{bi}))}$. By normalizing the capacitance change with incident photon flux $\Phi(E_\omega)$, we can express the spectrally resolved DLTS (SR-DLTS) signal as [21]

$$S(E_\omega) = \frac{C_0}{2N_i\Phi(E_\omega)}\sum_{j=1}^{N} N_t(t_j,E_\omega) = \frac{\overline{N}_t(E_\omega)}{2N_i\Phi(E_\omega)}C_0, \quad (7)$$

where the summation is taken over the time mesh of the optical irradiation duration, which overlaps with the sampling duration of capacitance-decaying curve. The light source employed for SR-DLTS is a monochromator-coupling 150 W tungsten–halogen light source wavelength tunable from 400 nm to 2 μm with 10-nm bandwidth.

2.2.3. Characterization of defect density in amorphous silicon films

For thin-film solar cells, the major limitation on PV efficiency is the trap-controlled transport. An AC-voltage capacitance measurement can provide the information about the total defect density $N_T = \sum_{E_t} N_t(E_t)$. This technique is known as drive-level capacitance profiling (DLCP) [22–24]. The nonlinear response of the capacitor as a function of the peak-to-peak voltage V_{pp} of an applied oscillating signal can be described as

$$C = C_0 + C_1 \cdot V_{pp} + C_2 \cdot (V_{pp})^2 + \cdots. \quad (8)$$

The density depth profile $N_T(w)$ that can be obtained from DLCP is given by $N_T(w) = -C_0^3/[2e\varepsilon_r\varepsilon_0 A^2 C_1]$ with $w = \varepsilon_r\varepsilon_0 A/C_0$.

To prepare a test sample for DLCP measurement, a 400-nm thick a-Si:H film was deposited on a highly doped P^+ Si crystal substrate at a temperature of 140 °C with ICP CVD or HF PECVD. The junction capacitance was then measured as a function of V_{pp} with different biased voltages to vary the thickness of the space charge region.

3. Results and discussion

3.1. Performances of a-Si pin solar cells

The current density–voltage (J–V) curves of a-Si pin solar cells prepared by ICP and VHF-PECVD are shown in Fig. 2(a). The dimensions and the i-layer thickness of the test cells are 1 cm × 1 cm and 400 nm, respectively. The J–V curve (solid squares) of the ICP a-Si solar cell indicates a PV conversion efficiency of 9.6% with a short-circuit current density of 15.7 mA/cm^2. Good-quality heavily doped p and n layers were fabricated successfully, resulting in an open-circuit voltage V_{oc} as high as 0.91 V. The low dark saturation current density 1.3×10^{-9} A/cm^2 (extracted from the dark J–V characteristics of the device) yields a fairly high fill factor (FF) of 67.2%. For comparison, the JV curve of VHF-PECVD a-Si solar cell (open

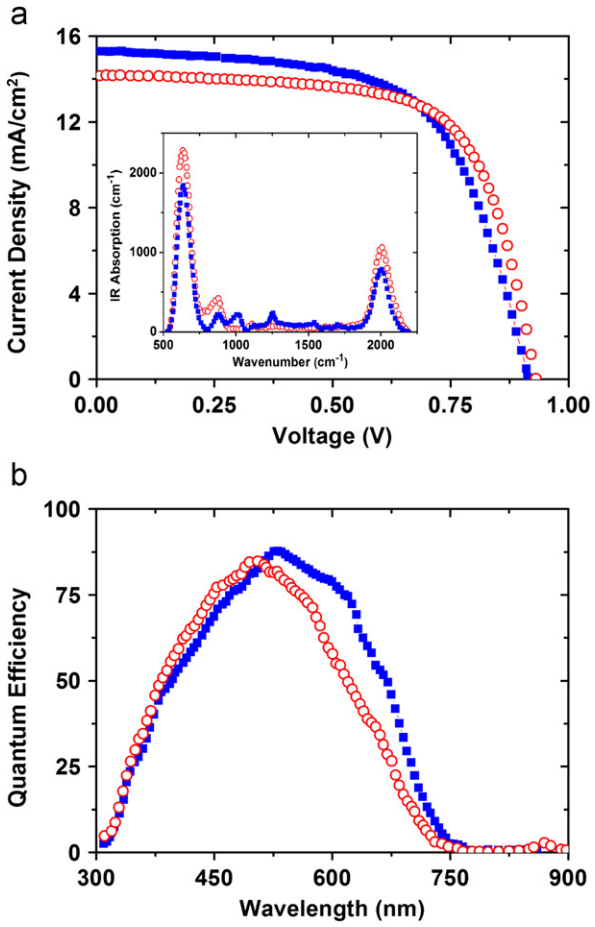

Fig. 2. (a) Current density versus voltage (J–V) characteristic curves of a-Si pin solar cells deposited by ICP-CVD (curve with blue solid squares) and VHF-PECVD (red open circles) at 140 °C. Inset showing the Fourier-transform infrared (FTIR) absorption spectra of 400-nm thick intrinsic a-Si layers deposited by the same methods. (b) The corresponding quantum-efficiency spectra of the same pin solar cells as used in (a). (For interpretation of the references to color in this figure legend, the reader is referred to the web version of this article.)

circles) reveals a conversion efficiency of 8.8% with V_{oc} (0.92 V) and FF (67.7%). The short-circuit current density is slightly lower (14.2 mA/cm^2) than that of the ICP device.

The quantum efficiency (QE) spectrum (solid squares) of the ICP cell shown in Fig. 2(b) covers 300–750 nm and slightly red shifts from that of the VHF-PECVD cell (open circles). It had been shown that a-Si film with lower hydrogen content has narrower bandgap and higher optical absorption than that with higher hydrogen inclusion [25]. The observed red-shift of the ICP QE spectrum suggests the hydrogen content of the ICP a-Si layer to be lower than that of the VHF-PECVD film. From the measured absorption edge profile, we determined the bandgap of our ICP a-Si film to be about 1.85 eV, which is slightly lower than 1.90 eV of VHF-PECVD films. To further verify the conjecture, we employed IR spectroscopy to determine the hydrogen content in the films. The FTIR spectra of a-Si:H films prepared by ICP (solid squares) and VHF-PECVD (open circles) are presented in the inset of Fig. 2(a). The absorption bands at around 640 cm^{-1} are related to the Si–H wagging mode. The stretching vibration modes corresponding to monohydride and dihydride bonding are present between 2000 and 2100 cm^{-1}. These silicon–hydrogen bonding types are often present in an amorphous silicon matrix and responsible for the degradation of the electrical properties of a-Si:H devices. The hydrogen content C_H can be determined by numerical integration of the Si–H wagging mode since the oscillator strength of this mode is independent of the preparation conditions and of the H content [26]. We estimated the hydrogen content of the ICP a-Si:H film to be about 9% and for the VHF-PECVD film $C_H \sim 12\%$. Therefore, we can attribute the higher short-circuit current density in the ICP a-Si solar cell shown in Fig. 2(a) to originate from higher optical absorption and lower defect density of the ICP a-Si layer.

3.2. Light-soaking test of a-Si pin solar cells

The major obstacle of amorphous Si PV technology is the low stability to optical irradiation, originating from generation of extra defects in a-Si by extended light exposure [5,7]. In Fig. 3(a), we found that the PV efficiency of the ICP a-Si solar cell drops by 12% (solid squares) from 9.6% to 8.5% after 10^4-s exposure at 60 °C with six-Sun. For the VHF-PECVD a-Si solar cell, the PV efficiency drops by 19% after 10^4-s exposure (open circles). The light soaking-induced changes in J–V curves were found mainly in a decrease of the fill factor and short-circuit current, suggesting new carrier losses being generated by light soaking.

3.3. Defect density and light-soaking test of a-Si:H layers

The defects in a thin-film solar cell can act as recombination centers of carriers, which reduce the carrier lifetime and form dipoles that further screen the electric field in the absorber layer of a solar cell. To clarify the underlying process of light soaking-induced degradation, we measured defect density of a-Si:H films as a function of exposure time with DLCP method [23]. For the measurements, 400-nm thick intrinsic a-Si:H films were deposited on P$^+$ c-Si substrate at 140 °C. In Fig. 3(b), we found that the ICP a-Si:H film has a defect density of 3×10^{15} cm^{-3}, while the VHF-PECVD a-Si:H layer has a slightly higher defect density 6×10^{15} cm^{-3}. The defect density of the ICP a-Si film increases to 1.5×10^{16} cm^{-3} after 10^4-s irradiation with six-Sun, comparing to 3.5×10^{16} cm^{-3} in the VHF-PECVD a-Si film under the identical condition.

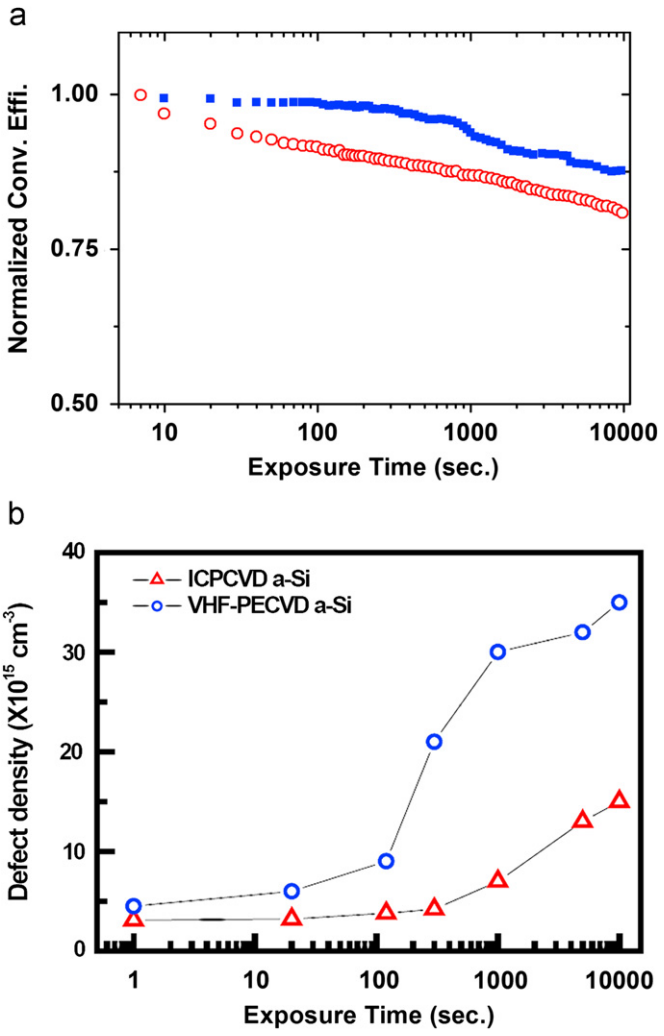

Fig. 3. (a) Conversion efficiency of a-Si:H pin solar cells grown by ICP-CVD (solid squares) and VHF-PECVD (open circles) as a function of exposure time with six-Sun light irradiance. (b) The defect densities retrieved from drive-level capacitance profile (DLCP) measurements of a-Si:H films deposited by ICP-CVD (open triangles) and VHF-PECVD (open circles) as a function of exposure time with the same light source as used in (a). The samples used were 400-nm thick intrinsic a-Si:H layers deposited on P$^+$ c-Si substrate at substrate temperature 140 °C.

3.4. Deep-level transient spectroscopy (DLTS) of ICP CVD a-Si:H solar cell

Deep level transient spectroscopy (DLTS) [27] is useful to identify the types of innate defects in a semiconductor film or newly generated by light soaking. In this study, we are interested to retrieve this important information from a working device. For this purpose, we prepared an ICP a-Si:H pin solar cell for the DLTS study. We reversely biased the device and then repetitively superimposed a pulse with appropriate duration on the DC bias to render the device into a brief forward bias condition. During the forward-bias duration, charge carriers were injected from both sides of the semiconductor junction into trap levels of the i-layer. Once the pulse is removed, the trapped carriers were emitted to the conduction/valence band of the i-layer with an emitting rate depending on the sample temperature. By using Eq. (4), N_t/N_i can be deduced and the resulting temperature profile of DLTS is presented in Fig. 4.

Two representative capacitance-decaying curves measured at 130 K and 300 K are shown in the inset of Fig. 4. From Eq. (4) and the observed positive decay amplitude $\Delta C(t)$, we concluded

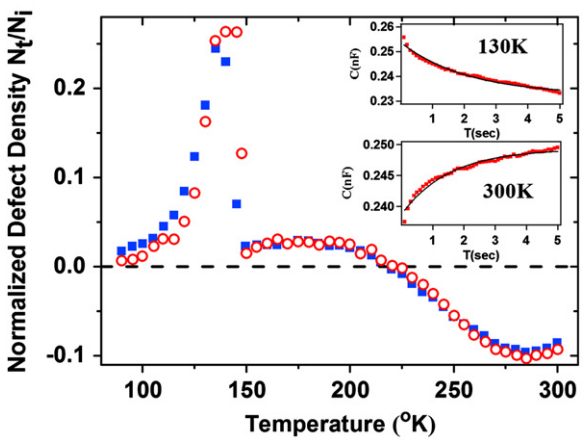

Fig. 4. Normalized defect densities retrieved from DLTS measurements on an as-deposited ICP a-Si pin solar cell (solid squares) and after 6.5-h light soaking (open circles) with 100 mW/cm^2 white light as a function of device temperature. Inset showing the corresponding decaying curves of the transient capacitance at 130 K and 300 K, respectively.

$N_t > 0$, implying that the positive peak at 130 K is generated by thermally activated hole-trapping defects. From 90 K to 150 K, the trapped holes at the defects have sufficient thermal energy to escape into the valence band and delocalize, resulting in a positive decaying capacitance curve. The negative peak near room temperature shall originate from electron-trapping defects lying below the conduction band edge with $E_c - E_t \simeq 35$ meV. These trapped electrons can escape into the conduction band near room temperature because they need higher thermal energy to conquer the trapping potential energy. Light soaking with 100 mW/cm^2 white light for 6.5 h (open circles) slightly modifies the distribution of the hole-trapping defects while leaves that of the electron-tapping defects nearly unaltered. For DLTS measurements at the device level, we used a much weaker light-soaking source than that used in Fig. 3(b), which was designed for accelerating test. The number of defects generated by light soaking is much smaller than that reported in Fig. 3(b). We estimated that the defect density of the device after light soaking shall remain about 3×10^{15} cm^{-3}.

Spectrally resolved DLTS technique [21] is useful for resolving the effect of light soaking on charge transport in an a-Si pin solar cell. For the spectrally resolved DLTS measurement, an optical radiation with photon energy E_ω illuminates the device during the DLTS data-taking period. The optically induced DLTS signal change $S(E_\omega)$ is obtained. In Fig. 5(a), the negative-valued $S(E_\omega)$ (open squares) at 90 K indicates $\overline{N}_t(E_\omega)$ to be negative, suggesting the optical transitions generate trapped electrons (see transition A of Fig. 5(b)). However, these trapped electrons do not have sufficient thermal energy to delocalize into the conduction band and thus effectively reduces the transient capacitance of the trapped holes from DLTS injection. Near room temperature, positive $S(E_\omega)$ (open circles) was observed, indicating $\overline{N}_t(E_\omega)$ to be positive. This suggests optical transitions increase the number of trapped holes (see transition B of Fig. 5(b)). The emission of the trapped holes into the valence band makes $\Delta C_{light}(t)$ less negative and therefore yields positive $S(E_\omega)$. As $E_\omega > 2.3$ eV, $S(E_\omega)$ starts to decrease. This is because the optical transition with $E_\omega > 2.3$ eV can raise the electron into the delocalized conduction band, thus reduces the DLTS sensitivity to light.

Based on the understanding of DLTS and SR-DLTS, we moved forward to resolve the effect of light soaking on charge transport in an a-Si pin solar cell. We irradiated the device with 100 mW/cm^2 white light for 1.5 and 6.5 h and then repeated the SR-DLTS measurements. The results are presented in Fig. 5(a) (see curves

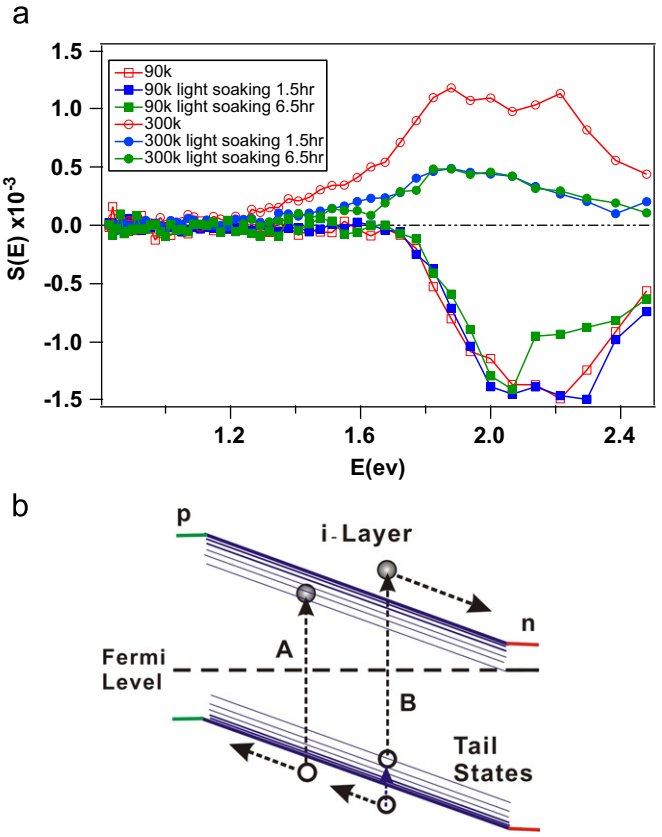

Fig. 5. (a) Spectrally resolved DLTS profiles of an ICP a-Si pin solar cell as a function of incident photon energy E_ω. The SR-DLTS profiles were measured at 90 K and 300 K on the as-deposited device as well as after 1.5 h and 6.5 h light soaking with 100 mW/cm^2 white light. (b) Schematic diagram depicting the optical transition occurring in SR-DLTS at 90 K (transition A) and 300 K (transition B).

with solid symbols). As shown at 90 K, light soaking effect on the SR-DLTS profile can only be observed near $E_\omega = 2.2$ eV. This can be understood by referring to Fig. 5(b), the trapped electrons generated by the optical transition A with $E_\omega = 2.2$ eV are close to the conduction band edge. Light soaking enhances the emission rate of the tapped electrons near the conduction band edge causing $S(E_\omega = 2.2\ \text{eV})$ to decrease. As noted above, at 300 K optical transition B generates trapped holes that yields positive $S(E_\omega)$. The major effect of light soaking on the hole-trapping defects is to reduce the transition moments $\langle c|\vec{r}|h\rangle$ from the hope-trapping defect levels $|h\rangle$ to the conduction band $|c\rangle$ so that $S(E_\omega)$ was found to decrease for 1.2 eV $\leq E_\omega = E_c - E_h \leq 2.5$ eV.

4. Conclusions

In summary, high-density ICP CVD technique had been successfully employed for fabricating solar cells with high conversion efficiency and light soaking stability. Single-junction a-Si pin solar cells with 400-nm thick i-layer achieved a conversion efficiency of 9.6%. We investigated light-soaking induced defects in the solar cells prepared by ICP CVD and VHF PECVD with defect-level capacitance profiling (DLCP), we found the defect level in the ICP CVD solar cell is lower and increases more slowly under six-Sun irradiation. Deep level transient spectroscopy (DLTS) revealed that the trapped holes near the valence band are delocalized at 130 K; while the trapped electrons can only be thermally delocalized near room temperature. Spectrally resolved DLTS study further indicates that light soaking enhances the emission rate of the tapped electrons near the

conduction band edge and reduces the transition moments from the hole-trapping defect levels to the conduction band. In addition to the increase of defect density revealed by DLCP, the combined effects are responsible to degrade the photovoltaic performance of a solar cell by light soaking. Our ICP CVD solar cell technology could offer a potential solution to low cost, high-efficiency PV with improved light-soaking stability. To further improve the light utilization efficiency for broad-band solar radiation, the ICP a-Si PV is also an ideal choice to integrate with other narrow bandgap materials to form multijunction devices.

Acknowledgments

The authors thank financial support from the National Science Council of the Republic of China under grant number of NSC97-2112-M009-006-MY3.

References

[1] F.J. Haug, T. Söderström, M. Python, V. Terrazzoni-Daudrix, X. Niquille, C. Ballif, Development of micromorph tandem solar cells on flexible low-cost plastic substrates, Solar Energy Materials & Solar Cells 93 (2009) 884–887.
[2] J.K. Rath, M. Brinza, Y. Liu, A. Borreman, R. Schropp, Fabrication of thin film silicon solar cells on plastic substrate by very high frequency PECVD, Solar Energy Materials & Solar Cells 94 (2010) 1534–1541.
[3] A.V. Shah, J. Meier, E. Vallat-Sauvain, N. Wyrsch, U. Kroll, C. Droz, U. Graf, Material and solar cell research in microcrystalline silicon, Solar Energy Materials & Solar Cells 78 (2003) 469–491.
[4] J. Meier, J. Spitznagel, U. Kroll, C. Bucher, S. Faÿ, T. Moriarty, A. Shah, Potential of amorphous and microcrystalline silicon solar cells, Thin Solid Films 451–452 (2004) 518–524.
[5] J. Poortmans, V. Arkhipov, Thin Film Solar Cell, John Wiley and Sons, Ltd., 2006.
[6] A. Matsuda, Thin-film silicon-growth process and solar cell application, Japanese Journal of Applied Physics 43 (2004) 7909–7920.
[7] A. Luque, S. Hegedus, Handbook of Photovoltaic Science and Engineering, John Wiley and Sons, Ltd., 2003.
[8] N. Kosku, F. Kurisum, M. Takegoshi, H. Takahashi, S. Miyazaki, High-rate deposition of highly crystallized silicon films from inductively coupled plasma, Thin Solid Films 435 (2003) 39–43.
[9] C. Niikura, N. Itagaki, M. Kondo, Y. Kawai, A. Matsuda, High-rate growth of microcrystalline silicon films using a high-density SiH_4/H_2 glow-discharge plasma, Thin Solid Films 457 (2004) 84–89.
[10] H. Jia, J.K. Saha, H. Shirai, Plasma parameters for fast deposition of highly crystallized microcrystalline silicon films using high-density microwave plasma, Japanese Journal of Applied Physics 45 (2006) 666–673.
[11] J. Wang, Y. Qin, H. Yan, P. Gao, J. Li, M. Yin, D. He, Columnar growth of crystalline silicon films on aluminum-coated glass by inductively coupled plasma CVD at room temperature, Chinese Physics B 18 (2009) 773–777.
[12] J. Li, J. Wang, M. Yin, D.H.P. Gao, Y.L.Q. Chen, H. Shirai, Deposition of controllable preferred orientation silicon films on glass by inductively coupled plasma chemical vapor deposition, Journal of Applied Physics 103 (2008) 043505 (7 pp.).
[13] J.H. Wu, J.M. Shieh, B.T. Dai, Y.C.S. Wu, Synthesis of microcrystalline silicon at room temperature using ICP, Electrochemical and Solid-State Letters 7 (2004) G128–G130.
[14] J.-M. Shieh, K.-C. Tsai, B.-T. Dai, Low hydrogen content in trimethylsilane-based dielectric barriers deposited by inductively coupled plasma, Applied Physics Letters 81 (2002) 1294–1296.
[15] J.H. Lim, K.N. Kim, J.K. Park, J.T. Lim, G.Y. Yeom, Uniformity of internal linear-type inductively coupled plasma source for flat panel display processing, Applied Physics Letters 92 (2008) 051504 (3 pp.).
[16] Y. Wu, M.A. Lieberman, The influence of antenna configuration and standing wave effects on density profile in a large-area inductive plasma source, Plasma Sources Science and Technology 9 (2000) 210.
[17] K.N. Kim, S.J. Jung, Y.J. Lee, G.Y. Yeom, S.H. Lee, J.K. Lee, Low-impedance internal linear inductive antenna for large-area flat panel display plasma processing, Journal of Applied Physics 97 (2005) 063302 (4 pp.).
[18] S. Mukhopadhyay, C. Das, S. Ray, Structural analysis of undoped microcrystalline silicon thin films deposited by PECVD technique, Journal of Physics D: Applied Physics 37 (2004) 1736.
[19] S.Y. Myong, O. Shevaleevskiy, K.S. Lim, S. Miyajima, M. Konagai, Charge transport in hydrogenated boron-doped nanocrystalline silicon–silicon carbide alloys, Journal of Applied Physics 98 (2005) 054311 (4 pp.).
[20] M. Lannoo, J. Bourgoin, Point Defects in Semiconductors, vol. 2, Experimental Aspects, Springer-Verlag, Berlin, 1981.
[21] J.D. Cohen, J.T. Heath, W.N. Shafarman, Photocapacitance spectroscopy in copper indium diselenide alloys, Springer Series in Materials Science 86 (2006) 69–90.
[22] S. Guha, J. Yang, D.L. Williamson, Y. Lubianiker, J.D. Cohen, A. Mahan, Structural, defect, and device behavior of hydrogenated amorphous Si near and above the onset of microcrystallinity, Applied Physics Letters 74 (1999) 1860–1862.
[23] T. Unold, J. Hautala, J.D. Cohen, Effect of carbon impurities on the density of states and the stability of hydrogenated amorphous silicon, Physical Review B 50 (1994) 16985–16994.
[24] E. Bhattacharya, A. Mahan, Microstructure and the light-induced metastability in hydrogenated amorphous silicon, Applied Physics Letters 52 (1988) 1587–1589.
[25] Y. Qin, H. Yan, F. Li, L. Qiao, Q. Liu, D. He, The optoelectronic properties of silicon films deposited by inductively coupled plasma CVD, Applied Surface Science 257 (2010) 817–822.
[26] U. Kroll, J. Meier, A. Shah, S. Mikhailov, J. Weber, Hydrogen in amorphous and microcrystalline silicon films prepared by hydrogen dilution, Journal of Applied Physics 80 (1996) 4971–4975.
[27] D.V. Lang, Deep-level transient spectroscopy: a new method to characterize traps in semiconductors, Journal of Applied Physics 45 (1974) 3023–3032.